Molecular Cell
Article

Genome-wide Measurement of RNA Folding Energies

Yue Wan,[1] Kun Qu,[1,8] Zhengqing Ouyang,[1,2,8] Michael Kertesz,[3] Jun Li,[4] Robert Tibshirani,[4] Debora L. Makino,[5] Robert C. Nutter,[6] Eran Segal,[7,*] and Howard Y. Chang[1,*]
[1]Howard Hughes Medical Institute and Program in Epithelial Biology
[2]Department of Genetics
Stanford University School of Medicine, Stanford, CA 94305, USA
[3]Howard Hughes Medical Institute and Department of Bioengineering
[4]Department of Statistics
Stanford University, Stanford, CA 94305, USA
[5]Department of Structural Cell Biology, Max Planck Institute of Biochemistry, D-82152 Martinsried, Germany
[6]Life Technologies, Foster City, CA 94404, USA
[7]Department of Computer Science and Applied Mathematics, Weizmann Institute of Science, Rehovot 76100, Israel
[8]These authors contributed equally to this work
*Correspondence: howchang@stanford.edu (H.Y.C.), eran@weizmann.ac.il (E.S.)
http://dx.doi.org/10.1016/j.molcel.2012.08.008

SUMMARY

RNA structural transitions are important in the function and regulation of RNAs. Here, we reveal a layer of transcriptome organization in the form of RNA folding energies. By probing yeast RNA structures at different temperatures, we obtained relative melting temperatures (Tm) for RNA structures in over 4000 transcripts. Specific signatures of RNA Tm demarcated the polarity of mRNA open reading frames and highlighted numerous candidate regulatory RNA motifs in 3′ untranslated regions. RNA Tm distinguished noncoding versus coding RNAs and identified mRNAs with distinct cellular functions. We identified thousands of putative RNA thermometers, and their presence is predictive of the pattern of RNA decay in vivo during heat shock. The exosome complex recognizes unpaired bases during heat shock to degrade these RNAs, coupling intrinsic structural stabilities to gene regulation. Thus, genome-wide structural dynamics of RNA can parse functional elements of the transcriptome and reveal diverse biological insights.

INTRODUCTION

Differential stability of RNA structures in the transcriptome corresponds to the diverse roles that RNA structures play in the cell. RNA structures can influence each step in the life cycle of a gene—from transcription, to pre-mRNA splicing, RNA transport, translation, and RNA decay (Wan et al., 2011). However, it is difficult to identify functional structural elements in the transcriptome because practically every RNA has the propensity to fold into extensive RNA structures. In addition to whether a base is paired, the stability of base pairing impacts the biological function of RNAs in important ways (Ringnér and Krogh, 2005). Some RNAs, such as ribozymes and structural RNA scaffolds (Guo et al., 2004; Wang and Chang, 2011); form stable secondary and tertiary structures; other RNAs, such as RNA thermometers and riboswitches, undergo structural rearrangements at specific temperatures or in the presence of ligands, respectively, to mediate gene regulation (Breaker, 2012; Chowdhury et al., 2006). As such, differential RNA stability is one way to distinguish diverse RNA structures and to identify functionally important elements in the transcriptome. While RNA folding energies are difficult to predict computationally because of contributions from complex tertiary RNA structures and ligand interactions (Wilkinson et al., 2005), RNA folding energies have been experimentally probed by measuring RNA Tm via several methods (Luoma et al., 1980; Rinnenthal et al., 2010; Wilkinson et al., 2005). Tm is defined as the temperature at which half of the molecules of a double-stranded species become single-stranded. RNA structures of low Tm are more dynamic and exhibit lower energetic cost to unwind and access; conversely, RNA structures of high Tm are relatively more stable and demand higher energetic cost to unfold.

We recently reported genome-wide RNA structure data for the yeast transcriptome by coupling RNA footprinting, using RNase V1 and S1 nuclease, to high-throughput sequencing (termed Parallel Analysis of RNA Structures, or PARS) (Kertesz et al., 2010). However, the relative stabilities of these structures and their influence on cellular biology remain unanswered. Inspired by the precedent of Tm measurement via RNA footprinting (e.g., SHAPE [Wilkinson et al., 2005]), here we directly measure the melting temperature at single nucleotide resolution across the yeast transcriptome. We coupled RNA footprinting using RNase V1 to high-throughput sequencing to probe for double-stranded regions across five temperatures, from 23 to 75 degrees Celsius (°C) (Figure 1A). This approach, termed Parallel Analysis of RNA structures with Temperature Elevation (PARTE), revealed the energetic landscape of the transcriptome and its multiple roles in posttranscriptional regulation.

RESULTS

Parallel Analysis of RNA Structures with Temperature Elevation

To carry out PARTE, we first defined conditions that allowed comparable results at different temperatures. RNA footprinting

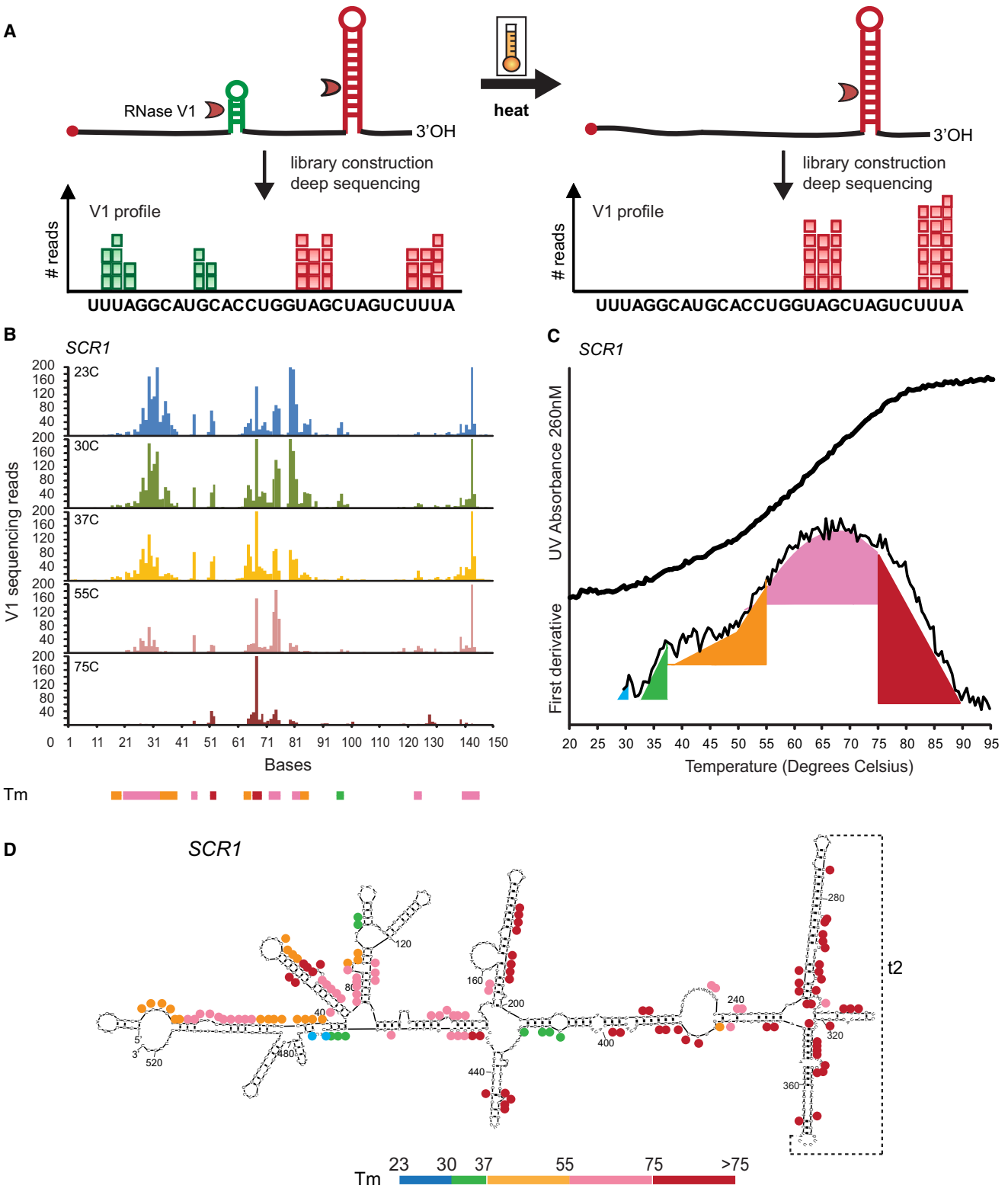

Figure 1. Measuring RNA Melting Temperatures by Deep Sequencing

(A) Schematic of PARTE experiment. Differential melting of RNA secondary structures is read out by deep sequencing of RNA fragments generated by double-stranded specific RNase V1. Each aligned sequence provides double-stranded structural information about a base (represented as a red or green square). A large number of reads aligned to a base indicates that the base was cleaved many times by RNase V1 and is hence more likely to be double stranded.

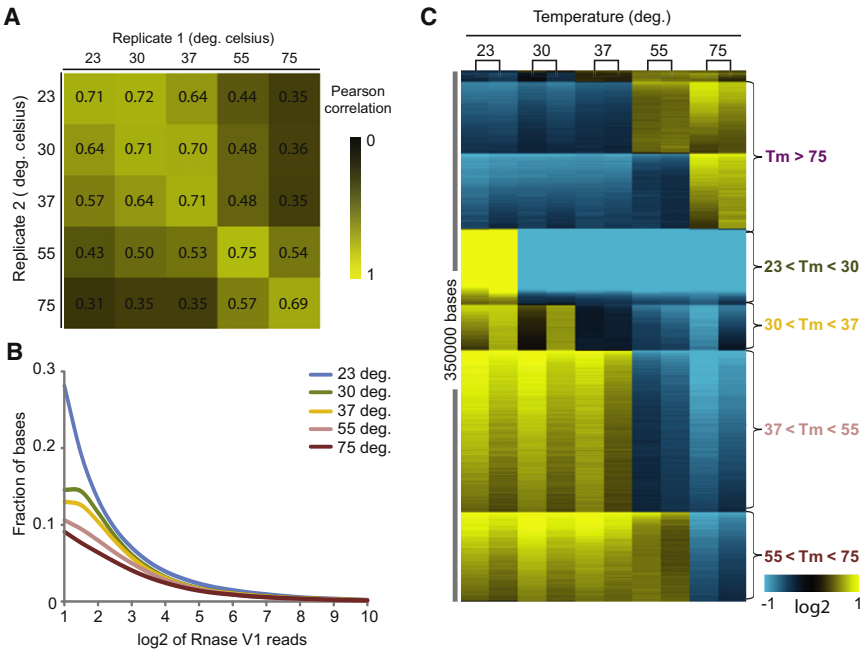

Figure 2. PARTE Identifies Melting Transitions at Single Nucleotide Resolution

(A) Pearson correlation of log2 of RNase V1 reads between biological replicates and samples of different temperatures. Biological replicates typically have the highest Pearson correlation (Pearson = 0.7). The greater the difference in temperature, the lower the Pearson correlation between two samples in their RNase V1 profile per base, which reflects the amount of pairing at that base.

(B) Distribution of RNase V1 cleavages with temperature. Bases with at least two RNase V1 reads at 23°C were analyzed for the distribution of RNase V1 reads with increasing temperature. In general, the percentage of bases with high V1 reads decreases with increasing temperature as more bases change from having V1 reads at 23°C to having low or no V1 reads at higher temperatures, indicating melting of RNA structures at higher temperatures.

(C) Temperature transition per base is identified using Stepminer program (Sahoo et al., 2007). Each row indicates the temperature at which RNase V1 cleavages transit from low to high or high to low reads. The two columns in each of the five temperatures are biological replicates. Blue indicates 2-fold decrease from the mean of normalized RNase V1 reads, and yellow indicates 2-fold increase from the mean of normalized RNase V1 reads.

with RNase V1 of the well-known structured domains of the Tetrahymena ribozyme (Guo et al., 2004) revealed that RNase V1 retains its double-stranded specificity up to 75°C, and comparable footprinting results were obtained at different temperatures by correspondingly shorter incubation times with the enzyme to maintain single-hit kinetics (Figure S1). Optimized conditions defined by these experiments were then used to probe RNA folding at different temperatures genome-wide. Next, we extracted total RNA from log-phase growth culture of yeast and performed polyA selection to enrich for mRNAs. Control RNAs, including domains of the *Tetrahymena* ribozyme and the human long noncoding RNAs HOTAIR and HOTTIP were added into the reactions (Rinn et al., 2007; Wang et al., 2011). The RNA pool was folded in vitro at 23°C and 30°C, and the 30°C pool was split and shifted to 30°C, 37°C, 55°C, or 75°C for 5 min. The RNA samples were then subjected to RNase V1 treatment with single-hit kinetics, and the resulting fragments were cloned for deep sequencing on the SOLiD platform as previously described (Kertesz et al., 2010) (Figure 1A). We performed two biological replicates for each temperature, yielding ten PARTE experiments in total. We generated over 3 million deep sequencing reads for each sample and mapped the reads to the yeast transcriptome to identify the cleavage sites (Table S1). Footprinting of the doped-in P4P6 domain of the *Tetrahymena* ribozyme showed that PARTE signals closely reproduced the traditional gel-based RNA footprint patterns across temperatures, indicating that the sequencing information accurately captures dynamic changes in RNA structure (Figure S1). We applied the PARTE data to examine the thermo-stability of the RNA subunit of the Signal Recognition Particle, *SCR1* (Figure 1B). Temperature transitions within local regions obtained by PARTE corresponded to those measured by UV spectroscopy (which detects base unstacking during melting of structured RNA) (Figure 1C) and identified differential stabilities of specific bases and helices in *SCR1* RNA structure (Figures 1D and S2). This provides a nucleotide resolution view of RNA structural stability, with each interrogated base serving as a probe of its local structural context.

PARTE Can Determine Melting Temperatures per Base

Pairwise comparison of all ten PARTE samples showed that biological replicates are most similar to each other, with a single exception, while the samples showed progressively more differences as the temperature gradation increased (Figure 2A). Analysis of data from all ten PARTE samples showed that stepwise increases in temperature led to stepwise losses of double-stranded regions, as expected (Figure 2B). We developed a computational procedure to infer Tm from PARTE data (Experimental Procedures). In brief, the data were normalized by the library sizes estimated by PoissonSeq (Li et al., 2012). Normalized data were fitted to an adaptive regression model to search

(B) Raw RNase V1 sequencing reads for the first 150 nt of the *SCR1* RNA at 23°C, 30°C, 37°C, 55°C, and 75°C. Regions that melt at different temperatures were shown as colored bars at the bottom of the graph. The colored bar indicates the last temperature that the structure was found stable.

(C) UV absorbance of full-length *SCR1* RNA at 260 nM, as well as first derivative of the UV absorbance over temperature, was obtained from 20°C–95°C. Nucleotide resolution melting transitions obtained by PARTE are indicated in color.

(D) RNA secondary structure of *SCR1* (Zwieb et al., 2005). A tertiary interaction is indicated as gray dotted lines. The melting transitions obtained from PARTE are indicated as colored dots.

for sharp transitions in read numbers at each base as a function of temperature ($p < 0.05$, FDR = 0.2, compared to running the same analysis on 100 permuted data sets) (Sahoo et al., 2007). Only bases that show a consistent single transition at a particular temperature across both biological replicates were included in downstream analysis. Indeed, single sharp transitions allowed an approximate Tm to be determined for more than 350,000 bases in the yeast transcriptome, mapping to 4016 distinct yeast mRNAs and 65 noncoding RNAs (Figure 2C). Approximately 80% of these bases had a transition from high RNase V1 reads to low V1 reads with temperature elevation (i.e., double-stranded RNA [dsRNA] became single stranded RNA [ssRNA]), with the majority of the bases melting between 37°C and 55°C (Figure 2C). Twenty percent of the Tm showed a transition for increased V1 reads at higher temperatures (55°C and 75°C); these bases likely represent sites in thermodynamically stable dsRNA structures, which were either increasingly sampled at higher temperatures as other paired bases melted away, or alternatively became accessible to RNase V1 upon dissolution of tertiary structures. We obtained an estimated melting temperature (eTm) per gene by averaging all the melting temperatures per base in that gene. Bases that do not melt by 75°C are assigned a Tm of 80°C for this calculation. To test the accuracy of our eTm, we determined the UV melting temperatures of twelve randomly chosen transcripts of approximately 100 bases, as UV spectrometry works best for short RNAs. Direct comparison of estimated Tm by PARTE versus UV spectroscopy for these RNAs showed good concordance (Spearman rank correlation, $R = 0.59$, $p < 0.05$); the concordance is even better for five of the transcripts with the most read coverage in PARTE data (>20% bases measured, Spearman rank correlation, $R = 0.9$, Figure S3A). These lines of evidence suggest that PARTE data are of good quality and are highly reproducible. PARTE estimates of Tm are demonstrably accurate at base resolution, and PARTE estimates of Tm per gene requires sufficiently deep sequence reads to generate transcript-wide coverage.

As another independent validation, we compared PARTE Tm to Tm predicted by computational algorithm. We used RNAFold (Gruber et al., 2008) to simulate the folding of the same set of yeast transcripts into secondary structures at 23°C, 30°C, 37°C, 55°C, or 75°C, and then extracted the Tm per base from the predicted secondary structures. Because secondary structure is one of the important building elements of folding energy, we expect that the predicted Tm will correlate to some degree with measured Tm, but will also deviate from the measured Tm because the algorithm does not model tertiary interactions. Indeed, we found that PARTE data is significantly correlated with computationally predicted Tm, but there are also substantial differences ($R = 0.24$, $p < 10^{-39}$, Figure S4). For the twelve transcripts where we determined Tm by UV spectroscopy, computational prediction correlated poorly with measured Tm (Spearman rank test, $R = -0.2$), performing substantially worse than PARTE. Thus, we suggest that PARTE data can be used in addition to computational algorithms to better estimate RNA folding energy.

PARTE Distinguishes Noncoding versus Coding RNAs

We first examined the thermodynamic properties of noncoding versus coding RNAs. Noncoding RNAs (ncRNAs) such as ribosomal RNAs, transfer RNAs, and RNase P are known to exhibit extensive secondary and tertiary structures of high stability (Clote et al., 2005). Indeed, the average melting profile of structured ncRNAs (rRNA, tRNA, snoRNA, and snRNA) is distinct from that of mRNAs (Figure 3A). While almost no base pairs in ncRNAs melted at $\leq$37°C, ~25% of bases in mRNAs melted by 37°C (odds ratio = 44:1, $p < 0.0001$, Fisher's exact test, for ncRNA over mRNA if <1% of bases in a transcript unpair at 30°C). ncRNAs also contain significantly more bases that remain paired at 75°C (odds ratio = 82:1, $p < 0.0001$, Fisher's exact test, for ncRNA over mRNA if $\geq$60% of bases remain paired at 75°C), which we term "stable bases." Noncoding RNAs also showed higher melting temperature per gene as compared to mRNAs ($p = 0.000018$, Wilcoxon rank sum test, Figure 3B), suggesting that ncRNAs contain more thermodynamically stable structures than mRNAs. We faithfully recapitulated the high structural stability of the Tetrahymena ribozyme in our data (Schultes et al., 2005; Szewczak et al., 1998) (Figure 3A). Two other yeast ncRNAs (*TLC1*, encoding telomerase RNA; *SCR1*, the RNA subunit of the Signal Recognition Particle) and the two doped-in human lincRNAs also show a profile that resembles the structured ncRNAs, indicating that structural stability may be a feature of some of these ncRNAs (Figure 3A). Interestingly, the noncoding RNA *SRG1*, a product of antisense transcription that silences *SER3* expression by transcription interference, has no known RNA function and showed a low stability profile that deviates from ncRNAs (Figure S3B). This example provides further support for the idea that PARTE can identify functional RNAs whose structures are important for their biological roles. The difference between mRNAs and functional ncRNAs persisted even if the untranslated regions (UTRs) of mRNAs were removed from consideration, and UTRs alone showed an intermediate profile between coding sequences and ncRNAs. The differing trend of RNA Tm for coding versus structured ncRNAs provides global experimental support for prior computational predictions (Clote et al., 2005).

Landscape of Melting Temperatures in Messenger RNAs Demarcates Open Reading Frames

Because PARTE identifies RNA Tm with nucleotide level resolution, we next addressed the energetic landscape across specific portions of mRNAs (Figure 4A). Previously, a static snapshot of global mRNA secondary structure showed that coding sequences (CDS) tend to be more structured than 5′ and 3′UTRs and that two regions with least stable base pairing—at the start and stop codons—demarcated the CDS (Kertesz et al., 2010). However, the symmetric pattern of RNA structural landscapes at start and stop codons raised the question of whether the structural landscapes of mRNA also encode the 5′ to 3′ polarity of translation. Alignment of PARTE profiles for mRNAs at the start and stop codons revealed a striking pattern that extended prior descriptions (Figures 4A–4C). First, the PARTE profiles confirmed the global pattern of RNA structure across functional portions of mRNAs, and confirmed predictions that UTRs are generally more accessible (Kertesz et al., 2010; Ringnér and Krogh, 2005). Second, the PARTE data showed that the two local regions with weakest pairings at start and stop codons are in fact flanked by diametrically opposite structural contexts.

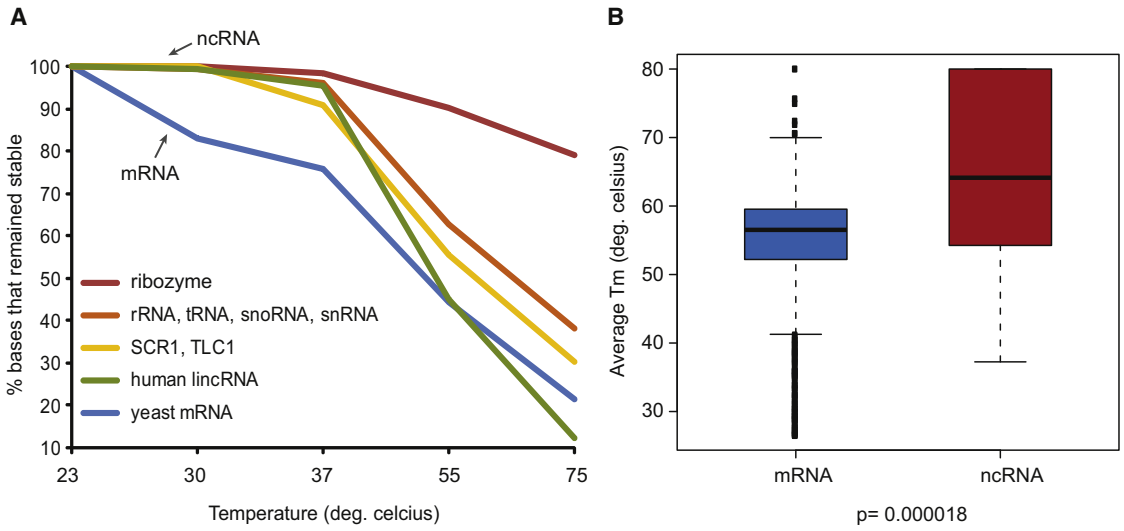

Figure 3. Different Classes of RNAs Can Be Classified according to Their Propensity to Melt

(A) The bases with confidently called Tms are separated into different classes of RNAs, which include coding, noncoding RNAs in the yeast transcriptome, human lincRNAs (fragments of HOTAIR and HOTTIP), and ribozymes (P4P6 and P9-9.2 domains of the Tetrahymena ribozyme). As shown in the graphs, mRNAs melt at lower temperatures than ncRNAs that often have structural roles.

(B) The estimated Tm of a gene was calculated as the average of all the Tm of the bases that belong to that gene. ncRNAs (red box) are significantly more thermostable than yeast mRNAs (blue box).

The most meltable part of the entire mRNA, on average, resides in nucleotides −3 to +3 surrounding the start codon. In contrast, the most stably paired region of the CDS maps to ~20 nucleotides immediately upstream and 10 nucleotides immediately downstream of the stop codon ($p < 0.01$ for each, permutation test, Figure 4C). This suggests the presence of a polarity in the energetic landscape of mRNA folding. Correlation of Tm with GC content showed that there is some correlation with GC content at the gene level ($R = 0.36$), however these Tm differences at the ends of mRNAs are not simply explained by GC content as meta-gene analysis of the GC content of these genes do not display the same polarity in base pairing as seen in RNA melting. This polarity of structure stability is hence likely to be consequences of secondary or higher order structures of RNAs that are directly detected by PARTE (Figures 4D and S4). Several reports have shown that both codon usage and RNA structure affects translation efficiency (Cannarozzi et al., 2010; Tuller et al., 2010). We and others have hypothesized that the 5′UTR immediately proximal to the start codon is the energetically most favorable portion of mRNAs, which may facilitate ribosome access. Consistent with this idea, we find a significant and positive correlation between the propensity of bases upstream of the start codon to melt and the translation efficiency of the gene (Figure 5B). In contrast, near the end of the open reading frame, it is possible that the ribosome can encounter a plateau of energetic barrier to unwind the RNA before it reaches the stop codon.

PARTE Nominates Numerous Functional Elements in the 3′UTR

To search for stable RNA structures within the yeast transcriptome, we identified continuous regions of RNA bases with Tm greater than 75°C. Consistent with the increased propensity to melt at the 5′UTR, we notice that on average, the 5′UTR contains fewer stable bases (1.3%), as compared to the coding region (19.7%) and 3′UTR (19.3%) (Figure 5A). Out of 820 5′UTRs for which we have Tm information, 35 contain stable bases, and they are significantly enriched in mRNAs that encode proteins localized to the cellular membrane ($p = 0.0017$) (Figure S5A). This finding raises the possibility that stable structures in the 5′UTR may serve as targeting signals to the membrane fraction of the cells, although they may also influence the translation efficiency of these genes as a class. Stable bases in the 3′UTR map to 337 genes, out of a total of 931 3′UTRs with Tm data, which is far more concentrated than expected by chance alone (Fisher's exact test, $p = 2.12 \times 10^{-67}$), suggesting that the stable bases in 3′UTR, if present, tend to be clustered and may encode regulatory RNA motifs. Indeed, ranking 3′UTRs by the length of continuous regions of stable base pairing in 3′ UTRs identified known functional structured RNA regulatory elements and nominated candidates in the yeast transcriptome, indicating the utility of our data set (Table S2).

The most stable RNA structure in 3′ UTRs is in *HAC1*, encoding a key transcription factor for the unfolded protein response (UPR) (Aragón et al., 2009); *HAC1* mRNA contains a stretch of 26 stable bases in its 3′ UTR (Figure 5C). Importantly, the region identified by our data coincides exactly with the structural RNA element required for *HAC1* mRNA localization to the ER membrane during heat shock, leading to *HAC1* mRNA splicing and protein production (Aragón et al., 2009) (Figure 5D). The second hit on our list is *RPS28B*, encoding a ribosomal protein which regulates its own mRNA level via decapping (Badis et al., 2004). *RPS28B* has a RNA structure in its 3′ UTR that is involved in recruiting decapping enzymes for

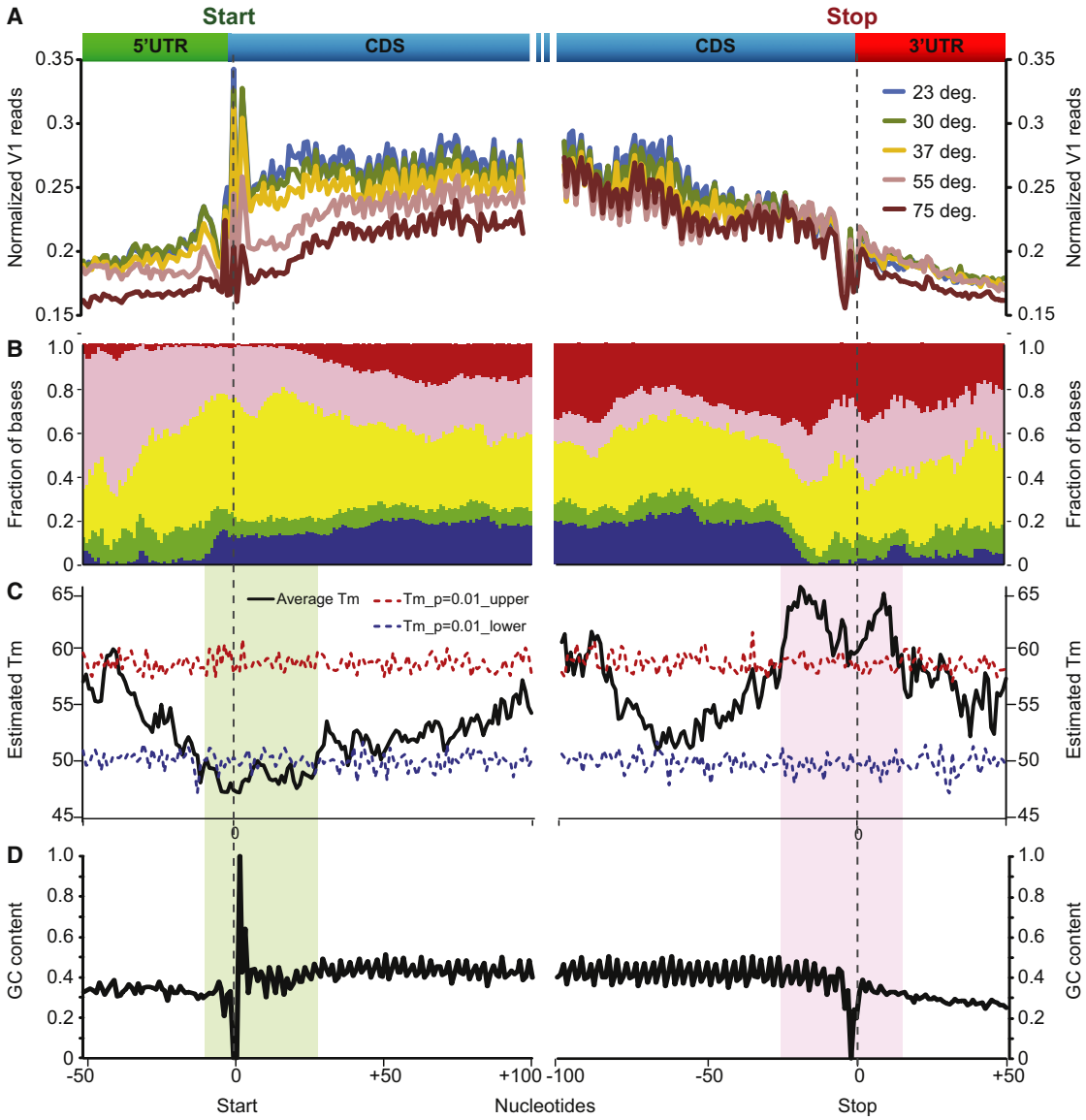

Figure 4. The Energetic Landscape of Messenger RNAs

(A) Normalized V1 reads were averaged across all mRNA transcripts that have at least 200 bases in their coding region and aligned by their start and stop codons (dotted brown lines).

(B) The relative abundance of bases with different Tms around the start (left) and stop (left) codon. The total number of Tm values at each position is normalized to 1.

(C) Average Tm profiles across 5′UTR, coding region, and 3′UTR. The −3 to +3nt region upstream of the start codon has the lowest average Tm, while the 20 nt upstream and 10 nt downstream of the stop codon has the highest Tm. The locations of the Tm values are randomized for 100 times along the gene body to obtain the null distributions of estimated Tms, which was used to calculate the p values. The dashed lines indicate the significance level of p = 0.01 (red: 1% chance of obtaining the observed or higher estimated Tm; blue: 1% chance of obtaining the observed or lower estimated Tm). The black line indicates the estimated Tm averaged across all the yeast genes for that particular base that is surrounding the translation start site (left) and the translation stop site (right).

(D) The average GC content around the translation start site (left) and the translation stop site (right).

mRNA degradation, and the region that we identified is immediately adjacent to this structure (Figure S5B). Moreover, stable RNA structures in 3′ UTRs may direct the cytotopic localization of mRNAs, an important mechanism for the cotranslational localization of proteins associated with membranes and organelles. Many genes with stable RNA structures in 3′ UTRs encode proteins that function in the endoplasmic reticulum membrane, Golgi apparatus, or the mitochondria (Table S2). These genes are significantly enriched for high membrane-to-free (MFI) index after cellular subfractionation, indicating that they are more likely to be membrane associated than cytoplasmic (Sylvestre et al., 2003) ($p < 0.05$, GSEA test

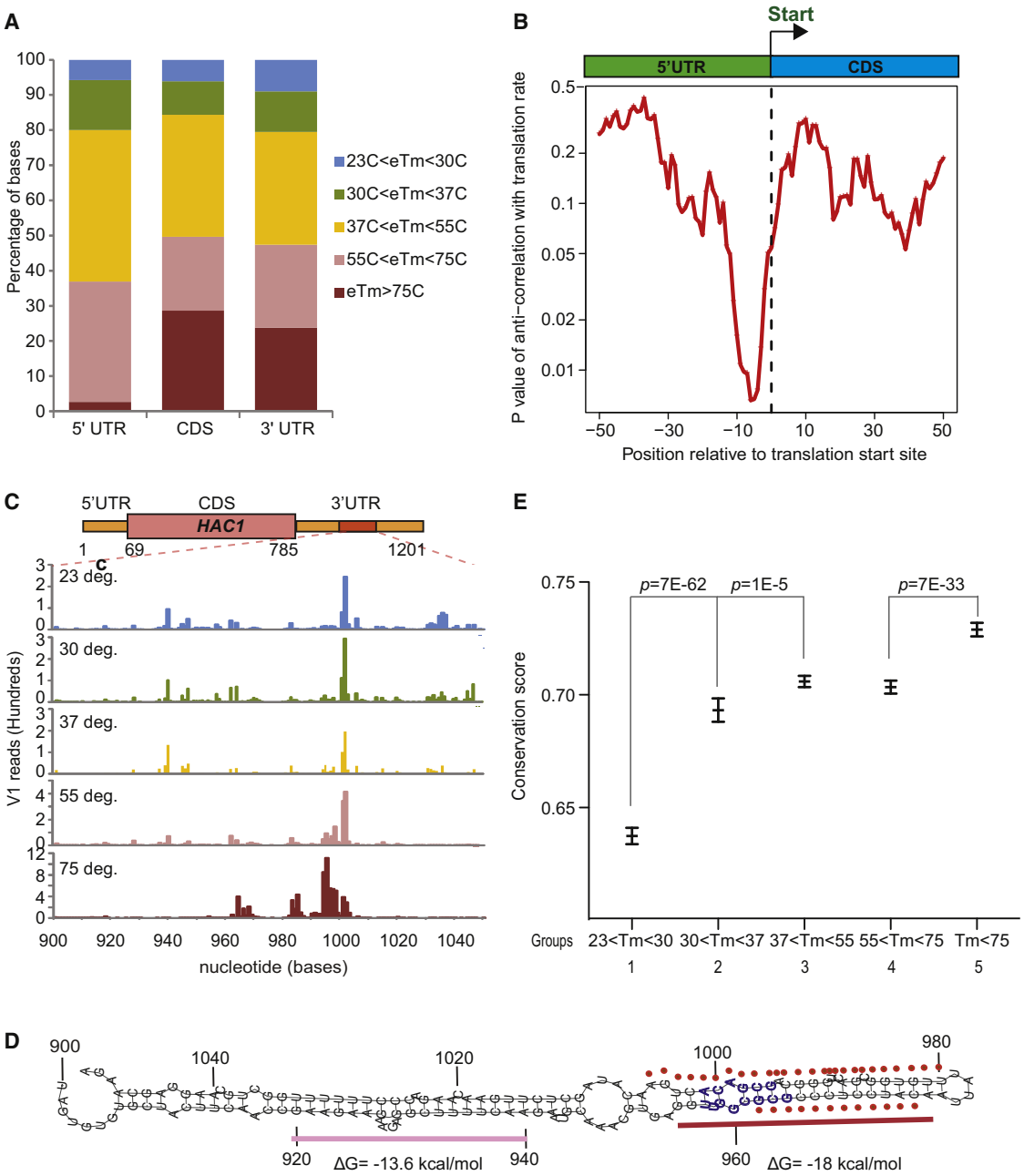

Figure 5. The Energetic Landscape of UTRs

(A) Distribution of Tm in 5′UTR, coding region, and 3′UTR. 5′UTRs have much less stable structures than coding regions or 3′UTRs.

(B) Thermal stability near the translation start codon is anticorrelated with translation rate. This small but significant anticorrelation of Tm over 23°C and the translation rate is centered on 10 bases upstream of the translation start site (R = 0.11, p = 0.007).

(C) High structural stability identifies RNA regulatory elements. The most stable element within 3′UTRs of yeast is nucleotides 900 to 1050 of *Hac1* mRNA; V1 reads are shown across the five temperatures. While many bases have RNase V1 cleavages at 23°C, only the region between 950 to 1100 nucleotides gained V1 reads at 75°C.

(D) Predicted secondary structure of nucleotides 900–1050 of *Hac1* mRNA. Bases with Tm > 75°C (red dots) are precisely the same region (blue bases) required for *Hac1* mRNA localization to the ER membrane during heat shock (Aragón et al., 2009). Although bases 955–975 and bases 920–940 are both double-stranded duplexes, the duplex 920–940 melted at lower temperatures than 955–975 as shown in D. ΔG for both duplexes were calculated (Dinamelt) and shown.

(E) Bases in high Tm structures are more conserved. An 11 nt moving window average of phastCons7way (7 yeast Multiz Alignment) for yeast (sacCer2 assembly) is calculated. For each population of bases (58772, 25721, 109324, 79496, and 66753 bases that melt by 30°C, 37°C, 55°C, 75°C and >75°C respectively), the mean and SEM were plotted using Prism program. More thermo-stable bases are significantly more conserved than meltable bases. We chose bases in CDS to eliminate biases that could occur due to more melting in the 5′UTRs.

[Subramanian et al., 2005]). Supporting the idea that stable bases are functional, these bases are also significantly more conserved across evolution than low Tm bases ($p < 10^{-20}$, student's t test, Figure 5E). Table S3 contains the entire list of stable base pairing in 3′ UTRs, as well as the precise location of candidate RNA motifs in each of these transcripts, which may serve as a useful resource as a starting point for finding localization and other structural elements in yeast mRNAs.

mRNAs with Low Melting Temperatures Are Enriched for Ribosomal Protein mRNAs

The energetic landscape of the transcriptome may facilitate the generation of diverse biological hypotheses. To identify functional classes enriched in genes with high or low eTm, we intersected sets of genes in the top 10 percentile (high) or bottom 10 percentile (low) eTm with Gene Ontology terms and genome-wide data sets of heat shock and RNA-binding proteins (Gasch et al., 2000; Hogan et al., 2008). Interestingly, low eTm genes are enriched for distinct functional classes, including ribosomal proteins (hypergeometric test, $p = 2.34 \times 10^{-74}$, FDR < 0.05), and targets of specific RNA-binding proteins (RBPs) (hypergeometric test, $p < 2 \times 10^{-4}$). The enrichment of ribosomal protein genes is not due to gene duplication ($p < 0.05$, FDR < 0.05 for all enrichments even if only one of two orthologs are considered), and gene location across the linear genome is not significantly clustered based on the eTm of the encoded transcripts.

RNA Melting Temperatures Inform Cellular Response to Heat Shock In Vivo

Importantly, mRNA folding energies in vitro is predictive of the pattern of RNA decay during heat shock in vivo. In bacteria, a key element of the heat shock response is "RNA thermometers"—RNA structures occluding ribosome binding sites in mRNAs of key regulators that melt at the heat shock temperature to enable protein synthesis (Chowdhury et al., 2006). The location and number of "RNA thermometers" in a eukaryote are not known. In yeast, we identified 25721 bases (7.4% of all measured) that specifically unpair upon a shift from 30°C to 37°C, which are clustered at more than 1800 sites in the transcriptome (Figure 6A and Table S4). These bases are enriched in the 5′ UTRs ($p < 2e\text{-}16$, chi-square test), and specifically around the ribosomal binding site, suggesting that some of these bases may also unpair during yeast heat shock to regulate translation (Figure 6B). Global gene expression profiling had identified gene sets that were induced or repressed in heat shock and other stresses (Gasch et al., 2000). Interestingly, our low eTm genes are highly enriched for these rapidly decreasing transcripts during the heat shock process (hypergeometric test, FDR < 0.05, p value of enrichment at 20, 30, 40, 60, and 80 min are 1×10^{-38}, 1×10^{-36}, 1×10^{-42}, 1×10^{-27}, and 1×10^{-4}, respectively) (Figure 6C). Interestingly, stratification of mRNAs by eTm over their lengths readily predicted the patterns of mRNA abundance during heat shock in vivo: mRNAs with the top quantile of eTm (most structurally stable) showed little decline in transcript level during heat shock, and mRNAs in quantiles of progressively lower eTm showed correspondingly larger and prolonged decreases in transcript levels (Figure 6D).

Structural Stability Regulates Heat Shock Induced mRNAs Decay by the Exosome

The ability of eTm to predict the pattern of heat shock induced RNA decay in vivo suggests that RNA structure modulates the activity of one or more components of the RNA decay machinery, a potentially new function of RNA thermometers. The exosome, the major 3′ to 5′ exonuclease in the cell, is a cage-like RNA processing machine; tunneling RNA into the exosome requires unpairing 31–33 nucleotides and is inhibited by structured RNAs with short 3′ overhangs (Bonneau et al., 2009). As such, we reasoned that the exosome is a good candidate for the factor that connects RNA thermometers to RNA decay. Indeed, exosome inactivation preferentially stabilized mRNAs with low eTm during heat shock, as shown by gene expression profiling (Figure 7A, 101 of 224 RNA thermometers stabilized versus 44.8 expected by chance alone, $p = 1.3 \times 10^{-22}$, hypergeometric test) (Gasch et al., 2000; Grigull et al., 2004; Houalla et al., 2006). mRNAs with progressively lower eTm are stabilized with greater magnitude in core exosome *rrp41-1* mutant (Figure 7B). The connection between the cytoplasmic core exosome and low eTm transcripts is highly specific. Deletion of nuclear exosome components *RRP6* failed to stabilize low eTm mRNAs, and deletion of *RRP47*, another nuclear exosome subunit, only increased the level these mRNAs at a late time point but did not prevent the initial decay (Figure 7A). Similarly, mutation of *CCR4* deadenylase stabilized many more transcripts, and showed weaker preference of whether the stabilized genes have low eTm and hence are easily degradable or not, as compared to the exosome complex (Figure S6). These results suggest that the exosome complex acts as a "reader" to discriminate between structured and unstructured substrates for decay in vivo.

To test if the structural stabilities of the RNAs is sufficient to determine RNA decay, we tested the ability of the ten-subunit *S. cerevisiae* exosome reconstituted from recombinant purified proteins to discriminate between endogenous RNAs with high and low eTms. *RPL1A* mRNA, encoding a ribosomal protein and with low eTm, is rapidly degraded by the exosome in 10 min, whereas *HAC1*, the key UPR activator and possessing a very stable 3′ UTR RNA structure (Figure 5D), is not processed by the exosome after 1 hr (Figure 7C). To further test the structural sensitivity of the exosome, we designed mutations to increase the structural stability of a model RNA hairpin (Dziembowski et al., 2007) in a stepwise fashion, which we confirmed by UV spectroscopy. RNA structures that are increasingly stable progressively blocked exosome processing (Figure 7D). Importantly, the exosome is active at 37°C to process a RNA hairpin engineered to melt between 30°C and 37°C, but not a RNA hairpin with higher Tm (Figure 7E). A structureless polyadenylate sequence is constitutively processed by the exosome at low and high temperatures (data not shown). Thus, the substrate preference of the exosome allows this complex to select different RNA structures in a temperature-dependent fashion.

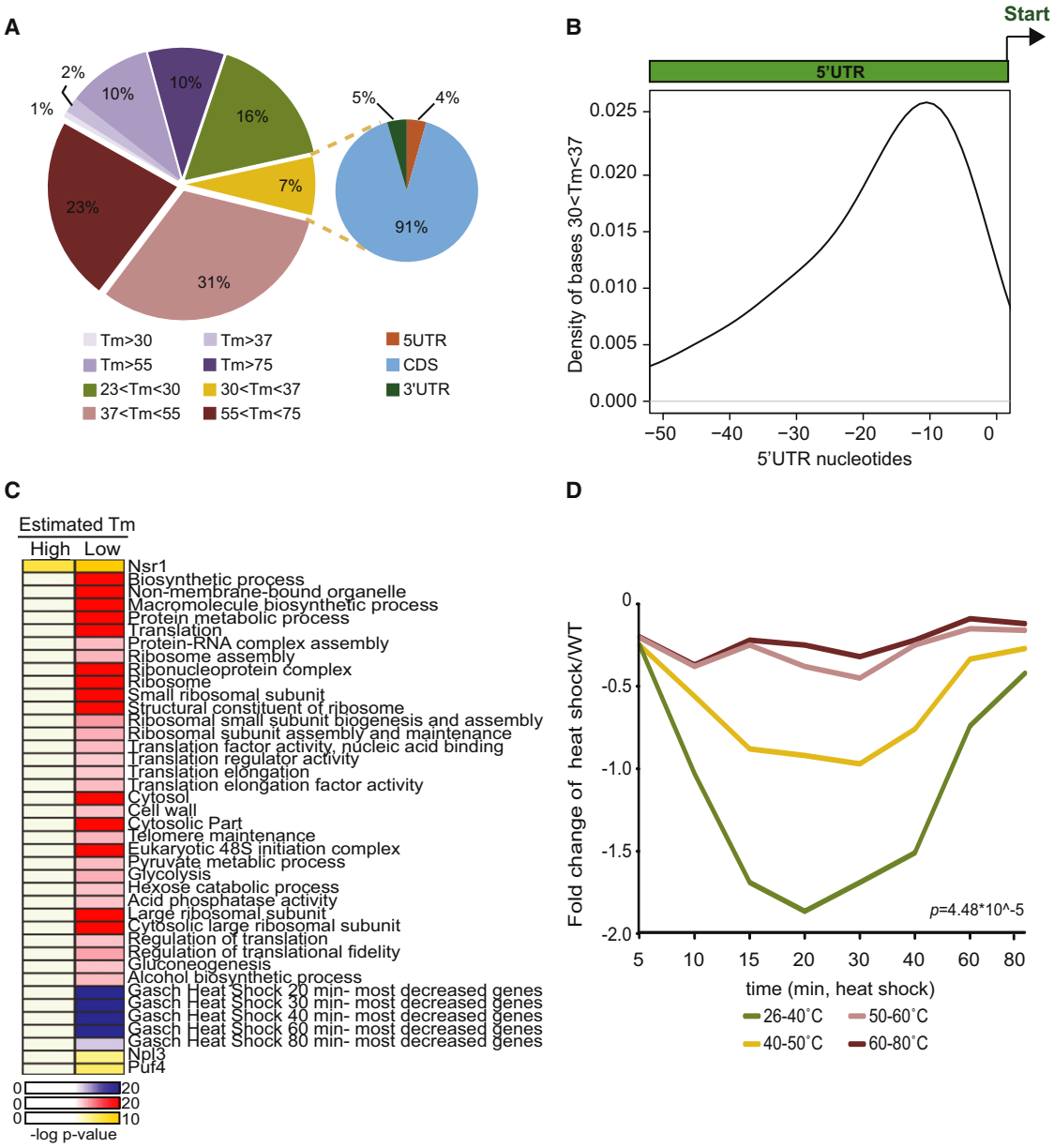

Figure 6. Functional Annotations of Genes with Low Estimated Melting Temperatures

(A) Distribution of bases that melt between 30°C to 37°C are among 5′UTR, CDS, and 3′UTR. Left: Distribution of melting temperatures in mRNA bases. Right: Distribution of bases that melt between 30°C –37°C.

(B) Bases that melt between 30°C –37°C in the 5′UTR are found most densely around ribosomal entry site (between −10 and −20 nt upstream of start codon). Tms are estimated by Stepminer.

(C) Enrichment of genes encoded by mRNAs with high or low melting temperatures in Gene Ontology (GO) terms (shown in red), interaction with specific RNA binding proteins (RBP, yellow), or regulation during heat shock (blue) (Gasch et al., 2000; Hogan et al., 2008). Genes are classified into the top or bottom 10 percentile according to their melting temperatures. Significance in overlap with gene sets is calculated using hypergeometric test (FDR < 0.05). mRNAs with low melting temperatures are significantly enriched for ribosomal components, in translation, bind to RBPs, as well as decrease greatly in abundance during heat shock.

(D) RNA folding energies predicts the pattern of RNA decay in vivo during heat shock. mRNAs were categorized according to their Tm. For each category, the median of their gene expression response to heat shock, along the time course, is plotted. Genes that fall into the different categories show significant differences in their response to heat shock ($p = 4.48 \times 10^{-5}$, ANOVA single factor analysis); genes with the lowest Tm show a most severe and sustained decrease during heat shock.

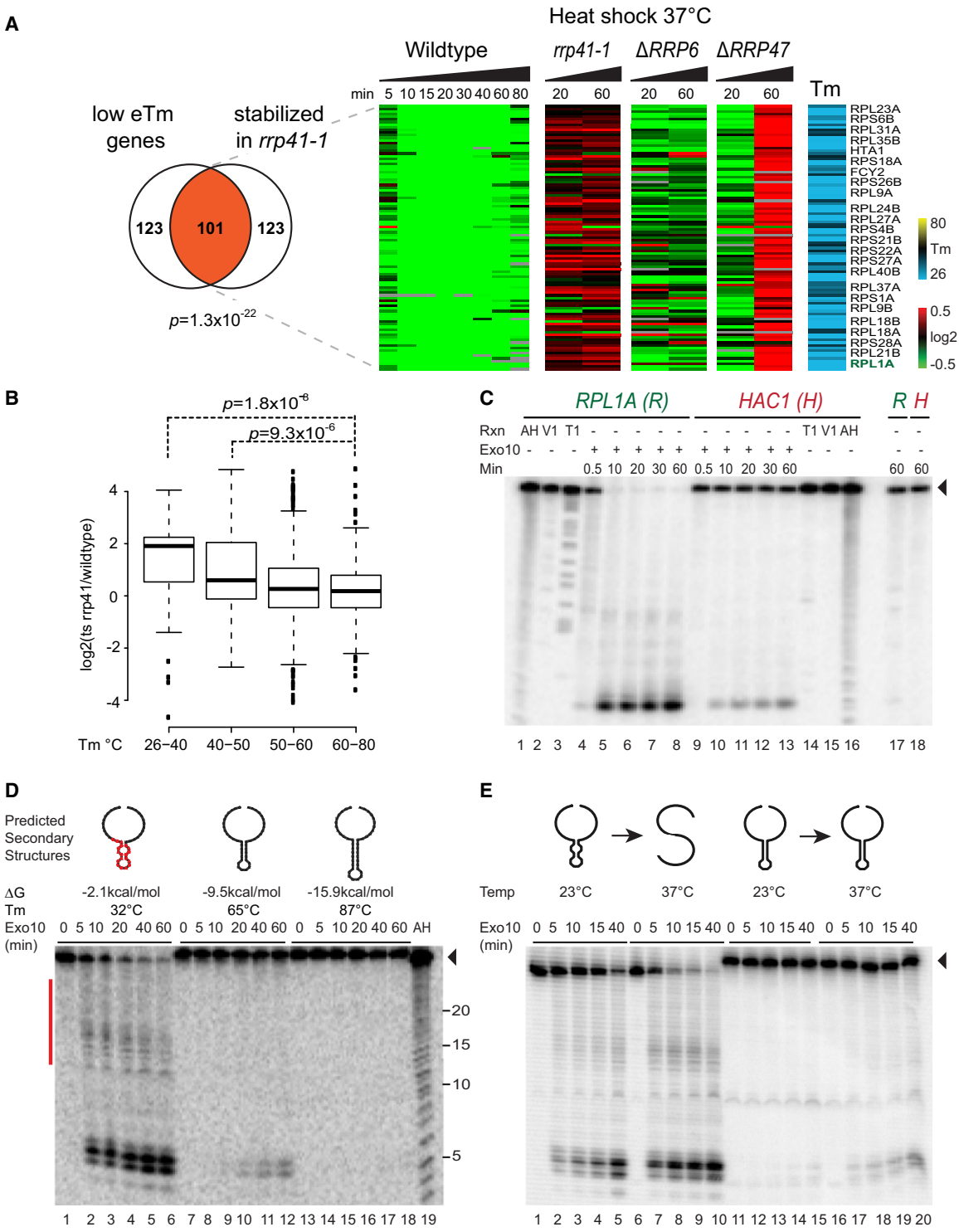

Figure 7. RNA Structure Stabilities Influence RNA Decay by Exosome Complex

(A) Exosome is required for selective heat-induced decay of low eTm transcripts. Left: Overlap of low eTm mRNAs and mRNAs stabilized genes in exosome *rrp41-1* mutant ($p = 1.3 \times 10^{-22}$, hypergeometric test). Right: Gene expression pattern of low Tm mRNAs during heat shock in WT versus mutant yeast. Each row is a gene, and each column indicates relative changes in transcript levels after heat shock as compared to WT yeast at room temperature. A low eTm mRNA, *RPL1A* (green), was randomly selected for biochemical studies in (C).

(B) Boxplot of genes in different eTm groups show that low eTm genes tend to be more stabilized in *rrp41-1* mutant at 20 min, 37°C. Stabilization is calculated by subtracting the log2 of gene expression change in WT yeast from log2 of gene expression change in *rrp41-1* yeast.

DISCUSSION

Genome-wide Measurement of RNA Melting Temperatures

By performing PARTE at several carefully calibrated temperatures, we have measured the relative stabilities of RNA structures in the yeast transcriptome. In essence, PARTE is the genome-scale version of the classical RNA melting experiments that characterizes energetics of RNA folding. PARTE provides complementary information to global RNA structural probing methods (Kertesz et al., 2010; Lucks et al., 2011; Underwood et al., 2010), and can potentially overcome some limitations of static RNase footprinting strategies. The impacts of sequence bias and steric hindrance, two concerns with several footprinting reagents, are minimized by focusing on condition-specific changes of signals that relate to RNA structure. Our results also demonstrate the feasibility of probing dynamic RNA structural transitions genome-wide, which can be extended to study the impact of specific proteins, small molecules, or conditions to yield functional information of RNAs in the cell. This work sets the ground for future improvements in coverage and accuracy. Because we performed polyA selection to enrich for mature abundant mRNAs in wild-type cells, introns and lowly expressed antisense or cryptic unstable transcripts were not well interrogated. Another important caveat of our procedure is that RNA structures requiring cotranscriptional folding or native protein-RNA interactions may not fold correctly, but our procedure preserves the in vivo pattern of RNA modifications (e.g., pseudouridines and methylated bases) that is difficult to reproduce with in vitro transcribed RNAs. We were able to accurately capture the known secondary structures of several yeast RNAs and Tetrahymena ribozyme added in as positive control (Kertesz et al., 2010). Classical studies of RNA folding energy are conducted in vitro, and we validated PARTE data with UV spectroscopy. Moreover, the ability of our Tm measurements to predict the pattern of heat-induced RNA decay in vivo and its regulation by the exosome demonstrate the physiological relevance of these findings. Finally, PARTE helps to infer but does not directly identify the base pairing partners; future efforts to combine PARTE with RNA mutagenesis may achieve this goal.

The genome-wide RNA Tm measurements provide a resource to annotate the transcriptome. By analyzing the patterns of RNA Tm, we found distinguishing features of RNA structural stability for several classes of transcripts and elements, including (i) coding versus noncoding RNAs, (ii) the beginnings and ends of open reading frames in mRNAs, (iii) candidate regulatory elements in 3′UTRs, and (iv) RNA thermometers associated with RNA decay during heat shock. Some of these features were previously predicted by computational analyses (Cannarozzi et al., 2010; Clote et al., 2005; Tuller et al., 2010), and our data provide genome-scale experimental support for them. Several of these findings were only evident based on genome-scale experimental data. Our data suggest that the transcriptome has evolved to possess extensive organization of its energetic landscape that can impact RNA cytotopic localization, translation, mRNA decay, and cellular response to stress.

RNA Tm as a Regulatory Signal in Heat Shock Response

The heat shock response is an evolutionarily conserved program for cells to adapt to temperature stress. Cells shut down general transcription and translation to decrease energy expenditure and accumulation of unfolded proteins, but need to selectively activate the UPR and produce heat shock proteins at the same time (Panniers, 1994). Our data indicate a role for RNA thermometers to direct RNA decay during heat shock. Messenger RNAs with low eTm, such as those encoding ribosomal proteins, are rapidly degraded during the heat shock while transcripts with higher eTm, such as key UPR activators *HAC1* and *PTC2,* are long lived. We found that the exosome preferentially degrades unpaired RNA and hence is the ''reader'' of the RNA thermometer. Moreover, exosome is selectively required for heat-induced RNA decay in vivo. Because exosome pausing would occur after mRNA deadenylation, our data raises the intriguing possibility of polyA independent translation, which can proceed efficiently in yeast (Brown and Johnson, 2001). Alternatively, deadenylated but not degraded mRNAs may also be readenylated by the protein CID13 for rapid gene expression (Saitoh et al., 2002). The low Tm genes, on the other hand, are rapidly turned over in heat shock to shut down translation. These results connect RNA structure, the exosome, and the physiology of the heat shock response. Notably, this regulatory information is apparently not determined by primary sequence motifs or specific secondary structures, but rather may be encoded in differences in RNA folding stabilities that is coordinately organized across the transcriptome.

EXPERIMENTAL PROCEDURES

PARTE

Total RNA was extracted from log phase S288C yeast using a slightly modified protocol that uses hot acid phenol (Sigma). Poly(A) RNA was obtained by purifying twice using the Poly(A) purist MAG Kit according to the manufacturer's instructions (Ambion). RNA transcripts of the P4P6 and P9-9.2 domains of the Tetrahymena ribozyme and fragments of HOTAIR and HOTTIP are obtained by PCR followed by in vitro transcription using RiboMAX Large Scale RNA production Systems Kit according to the manufacturer's instructions

(C) Exosome reads endogenous RNA thermometers. Ten-subunit exosome complex (Exo10) selectively degrades a 150-mer fragment of *RPL1A* (Tm of gene = 29°C) over a 150-mer fragment of *HAC1* (Tm of gene = 62°C). Full-length substrate (black arrowhead). RNA treatment with alkaline hydrolysis (AH, lanes 1 and 16), RNase V1 (lanes 2 and 15), and RNase T1 in 8 M urea (lanes 3 and 14) are shown. RNA substrates were stable in the absence of Exo10 for 60 min at 37°C (lanes 17 and 18).

(D) RNA secondary structure blocks exosome processing. Exo-10 reaction with designer substrates with increased pairing stability (44-mer substrate [Dziembowski et al., 2007], 44mut2, 44mut4); substrate Tms were measured by UV spectrometry. The red bar indicates the residues that Exo10 partially stops at and are mapped to the stem loop (red) in the predicted secondary structure of the 44-mer RNA.

(E) Recapitulation of heat-induced RNA decay by the exosome. Exo10 (2 nM) was incubated with 100 nM of 44-mer RNA or 44mut2 RNA subtrate at 37°C. The 44-mer substrate functions as a RNA thermometer; its unpairing at 37°C facilitates decay by Exo10. In contrast, mutations that raise the Tm in 44mut2 render it nondegradable by Exo10 at 37°C.

(Promega) and purified by PAGE purification. P4P6, P9-9.2, and fragments of HOTAIR and HOTTIP were doped into 2 μg of yeast poly(A)$^+$ mRNA as controls. Briefly, the RNAs were heated to 90°C for 2 min, cooled on ice for 2 min and incubated at 23°C for 20 min, after adding 10X RNA structure buffer. The RNA pool is then probed using 0.005 U of RNase V1 in 100 ul reaction volume for 15 min at 23°C.

The RNA pool to be shifted to different temperatures was heated to 90°C for 2 min, cooled on ice for 2 min, and slowly brought to 30°C in RNA structure buffer for 15 min. The RNA pool was then either structure probed at 30°C using RNase V1(Ambion) or shifted to 37°C, 55°C, or 75°C for 5 min before undergoing structure probing at the respective temperatures using RNase V1. RNase V1 in 0.04 U, 0.028 U, 0.014 U, and 0.005 U was added at 30°C, 37°C, 55°C, and 75°C, respectively, for 1min. The nuclease reactions were inactivated and precipitated using an inactivation and precipitation buffer (Ambion). RNA ligation to SOLiD adaptors, amplification, and sequencing were as described (Kertesz et al., 2010) and detailed in Supplemental Experimental Procedures. The mapping results are provided in Table S1.

Data Analysis

PARTE data normalization, Tm estimation, and genomic analyses are detailed in Supplemental Experimental Procedures.

RNA Footprinting of Radio-Labeled RNA

In vitro transcribed RNA was 5′end labeled with γP32 ATP using T4 PNK kinase (NEB) as previously described. The radio-labeled RNA was structure probed with RNase V1 in 1 ug of poly(A)$^+$ RNA at different temperatures as described below and in Supplemental Experimental Procedures.

UV Spectroscopy

Yeast genes (SCR1, snR52, YCR024C-A, RDN58-1, YER138W-A, snR60, snR68, snR75, snR24, snR39B, snR18, and snR13), as well as P9-9.2 domain of Tetrahymena ribozyme, were PCR amplified and in vitro transcribed. Each RNA was heat denatured at 90°C for 5 min in 900 ul of water, snap cooled on ice for 10 min before adding 100 ul of 10X buffer (100 mM sodium cacodylate [pH7], 5 mM MgCl2, 1M KCl) and incubating the RNA at room temperature for 30 min. UV absorbance was obtained by heating the RNA from 20°C–95°C using Cary 100 Bio UV-vis spectrometer at 1°C/min. Readings were taken at 260 nM every 0.5 min. Tm is predicted from curve fitting in Meltwin 3.0 program using the "non-self complementary" parameter. First derivative is obtained using KaleidaGraph and smoothed in Excel by taking a moving window of 20 data points.

Exosome Assay

Two 150-mer fragments near the 3′ end of *RPL1A* and *HAC1* gene respectively were PCR amplified and in vitro transcribed. The 44-mer RNA substrate was chemically synthesized (Dziembowski et al., 2007). Two point mutations were made to stabilize the stem loop structure in the RNA (44mut2); two more point mutations were made to lengthen the stem loop (44mut4). Melting temperatures of 44-mer RNA constructs were obtained using UV absorbance by heating the RNA from 20°C–95°C, at 1°C/min, in buffer (final concentration: 50 mM HEPES [pH7.5], 50 mM NaCl, 200 uM Mg Acetate). Sequences of RNA substrates can be found in Supplemental Experimental Procedures. 5′end labeled RNA was heated to 90°C for 2 min, snap cooled on ice for 2 min, and incubated with exosome reaction buffer (final concentration: 50 mM HEPES [pH7.5], 50 mM NaCl, 200 uM MgAcetate, 10% Glycerol, 0.1%NP40, 1mM DTT) (Bonneau et al., 2009) at room temperature for 20 min before adding exosome (Exo-10) to final 10 ul reaction. At indicated time points, 2 ul aliquots were taken, and the reaction was quenched by adding 8 ul of RNA loading dye II (Ambion). The reaction products were resolved on a 15% TBE-urea PAGE gel and visualized by phosphorimaging.

ACCESSION NUMBERS

The GEO accession number is GSE39680.

SUPPLEMENTAL INFORMATION

Supplemental Information includes six figures, four tables, Supplemental Experimental Procedures, and Supplemental References and can be found with this article online at http://dx.doi.org/10.1016/j.molcel.2012.08.008.

ACKNOWLEDGMENTS

We thank G. Sherlock, K. Schwartz, E.T. Kool, A.R. Hernández, W. Greenleaf, G. Zheng, B. Batista, M.C. Tsai, M.H. Tan, and the Life Technologies SOLiD team for assistance and critiques. We thank E. Conti for insights and support for the exosome experiment. This work was supported by a National Institutes of Health grant (R01-HG004361). Y.W. is funded by the Agency of Science, Technology, and Research of Singapore. E.S. is the incumbent of the Soretta and Henry Shapiro career development chair. H.Y.C. is an Early Career Scientist of the Howard Hughes Medical Institute. Y.W., M.K., H.Y.C., and E.S. conceived the project; Y.W. and H.Y.C. developed the protocol and designed the experiments; Y.W. performed all experiments; Y.W., K.Q., Z.O., M.K., J.L., R.T., E.S., and H.Y.C. planned and conducted the data analysis; D.L.M. and E.C. provided the reconstituted exosome complex; R.C.N. helped with sequencing; Y.W. and H.Y.C. wrote the paper with contributions from all authors.

Received: April 6, 2012
Revised: June 19, 2012
Accepted: August 2, 2012
Published online: September 13, 2012

REFERENCES

Aragón, T., van Anken, E., Pincus, D., Serafimova, I.M., Korennykh, A.V., Rubio, C.A., and Walter, P. (2009). Messenger RNA targeting to endoplasmic reticulum stress signalling sites. Nature *457*, 736–740.

Badis, G., Saveanu, C., Fromont-Racine, M., and Jacquier, A. (2004). Targeted mRNA degradation by deadenylation-independent decapping. Mol. Cell *15*, 5–15.

Bonneau, F., Basquin, J., Ebert, J., Lorentzen, E., and Conti, E. (2009). The yeast exosome functions as a macromolecular cage to channel RNA substrates for degradation. Cell *139*, 547–559.

Breaker, R.R. (2012). Riboswitches and the RNA World. Cold Spring Harb. Perspect. Biol. *4*, a003566.

Brown, J.T., and Johnson, A.W. (2001). A cis-acting element known to block 3′ mRNA degradation enhances expression of polyA-minus mRNA in wild-type yeast cells and phenocopies a ski mutant. RNA *7*, 1566–1577.

Cannarozzi, G., Schraudolph, N.N., Faty, M., von Rohr, P., Friberg, M.T., Roth, A.C., Gonnet, P., Gonnet, G., and Barral, Y. (2010). A role for codon order in translation dynamics. Cell *141*, 355–367.

Chowdhury, S., Maris, C., Allain, F.H., and Narberhaus, F. (2006). Molecular basis for temperature sensing by an RNA thermometer. EMBO J. *25*, 2487–2497.

Clote, P., Ferré, F., Kranakis, E., and Krizanc, D. (2005). Structural RNA has lower folding energy than random RNA of the same dinucleotide frequency. RNA *11*, 578–591.

Dziembowski, A., Lorentzen, E., Conti, E., and Séraphin, B. (2007). A single subunit, Dis3, is essentially responsible for yeast exosome core activity. Nat. Struct. Mol. Biol. *14*, 15–22.

Gasch, A.P., Spellman, P.T., Kao, C.M., Carmel-Harel, O., Eisen, M.B., Storz, G., Botstein, D., and Brown, P.O. (2000). Genomic expression programs in the response of yeast cells to environmental changes. Mol. Biol. Cell *11*, 4241–4257.

Grigull, J., Mnaimneh, S., Pootoolal, J., Robinson, M.D., and Hughes, T.R. (2004). Genome-wide analysis of mRNA stability using transcription inhibitors and microarrays reveals posttranscriptional control of ribosome biogenesis factors. Mol. Cell. Biol. *24*, 5534–5547.

Gruber, A.R., Lorenz, R., Bernhart, S.H., Neuböck, R., and Hofacker, I.L. (2008). The Vienna RNA websuite. Nucleic Acids Res. *36* (Web Server issue), W70–4.

Guo, F., Gooding, A.R., and Cech, T.R. (2004). Structure of the Tetrahymena ribozyme: base triple sandwich and metal ion at the active site. Mol. Cell *16*, 351–362.

Hogan, D.J., Riordan, D.P., Gerber, A.P., Herschlag, D., and Brown, P.O. (2008). Diverse RNA-binding proteins interact with functionally related sets of RNAs, suggesting an extensive regulatory system. PLoS Biol. *6*, e255.

Houalla, R., Devaux, F., Fatica, A., Kufel, J., Barrass, D., Torchet, C., and Tollervey, D. (2006). Microarray detection of novel nuclear RNA substrates for the exosome. Yeast *23*, 439–454.

Kertesz, M., Wan, Y., Mazor, E., Rinn, J.L., Nutter, R.C., Chang, H.Y., and Segal, E. (2010). Genome-wide measurement of RNA secondary structure in yeast. Nature *467*, 103–107.

Li, J., Witten, D.M., Johnstone, I.M., and Tibshirani, R. (2012). Normalization, testing, and false discovery rate estimation for RNA-sequencing data. Biostatistics *13*, 523–538.

Lucks, J.B., Mortimer, S.A., Trapnell, C., Luo, S., Aviran, S., Schroth, G.P., Pachter, L., Doudna, J.A., and Arkin, A.P. (2011). Multiplexed RNA structure characterization with selective 2′-hydroxyl acylation analyzed by primer extension sequencing (SHAPE-Seq). Proc. Natl. Acad. Sci. USA *108*, 11063–11068.

Luoma, G.A., Burns, P.D., Bruce, R.E., and Marshall, A.G. (1980). Melting of Saccharomyces cerevisiae 5S ribonucleic acid: ultraviolet absorption, circular dichroism, and 360-MHz proton nuclear magnetic resonance spectroscopy. Biochemistry *19*, 5456–5462.

Panniers, R. (1994). Translational control during heat shock. Biochimie *76*, 737–747.

Ringnér, M., and Krogh, M. (2005). Folding free energies of 5′-UTRs impact post-transcriptional regulation on a genomic scale in yeast. PLoS Comput. Biol. *1*, e72.

Rinn, J.L., Kertesz, M., Wang, J.K., Squazzo, S.L., Xu, X., Brugmann, S.A., Goodnough, L.H., Helms, J.A., Farnham, P.J., Segal, E., and Chang, H.Y. (2007). Functional demarcation of active and silent chromatin domains in human HOX loci by noncoding RNAs. Cell *129*, 1311–1323.

Rinnenthal, J., Klinkert, B., Narberhaus, F., and Schwalbe, H. (2010). Direct observation of the temperature-induced melting process of the Salmonella fourU RNA thermometer at base-pair resolution. Nucleic Acids Res. *38*, 3834–3847.

Sahoo, D., Dill, D.L., Tibshirani, R., and Plevritis, S.K. (2007). Extracting binary signals from microarray time-course data. Nucleic Acids Res. *35*, 3705–3712.

Saitoh, S., Chabes, A., McDonald, W.H., Thelander, L., Yates, J.R., and Russell, P. (2002). Cid13 is a cytoplasmic poly(A) polymerase that regulates ribonucleotide reductase mRNA. Cell *109*, 563–573.

Schultes, E.A., Spasic, A., Mohanty, U., and Bartel, D.P. (2005). Compact and ordered collapse of randomly generated RNA sequences. Nat. Struct. Mol. Biol. *12*, 1130–1136.

Subramanian, A., Tamayo, P., Mootha, V.K., Mukherjee, S., Ebert, B.L., Gillette, M.A., Paulovich, A., Pomeroy, S.L., Golub, T.R., Lander, E.S., and Mesirov, J.P. (2005). Gene set enrichment analysis: a knowledge-based approach for interpreting genome-wide expression profiles. Proc. Natl. Acad. Sci. USA *102*, 15545–15550.

Sylvestre, J., Vialette, S., Corral Debrinski, M., and Jacq, C. (2003). Long mRNAs coding for yeast mitochondrial proteins of prokaryotic origin preferentially localize to the vicinity of mitochondria. Genome Biol. *4*, R44.

Szewczak, A.A., Podell, E.R., Bevilacqua, P.C., and Cech, T.R. (1998). Thermodynamic stability of the P4-P6 domain RNA tertiary structure measured by temperature gradient gel electrophoresis. Biochemistry *37*, 11162–11170.

Tuller, T., Waldman, Y.Y., Kupiec, M., and Ruppin, E. (2010). Translation efficiency is determined by both codon bias and folding energy. Proc. Natl. Acad. Sci. USA *107*, 3645–3650.

Underwood, J.G., Uzilov, A.V., Katzman, S., Onodera, C.S., Mainzer, J.E., Mathews, D.H., Lowe, T.M., Salama, S.R., and Haussler, D. (2010). FragSeq: transcriptome-wide RNA structure probing using high-throughput sequencing. Nat. Methods *7*, 995–1001.

Wan, Y., Kertesz, M., Spitale, R.C., Segal, E., and Chang, H.Y. (2011). Understanding the transcriptome through RNA structure. Nat. Rev. Genet. *12*, 641–655.

Wang, K.C., and Chang, H.Y. (2011). Molecular mechanisms of long noncoding RNAs. Mol. Cell *43*, 904–914.

Wang, K.C., Yang, Y.W., Liu, B., Sanyal, A., Corces-Zimmerman, R., Chen, Y., Lajoie, B.R., Protacio, A., Flynn, R.A., Gupta, R.A., et al. (2011). A long noncoding RNA maintains active chromatin to coordinate homeotic gene expression. Nature *472*, 120–124.

Wilkinson, K.A., Merino, E.J., and Weeks, K.M. (2005). RNA SHAPE chemistry reveals nonhierarchical interactions dominate equilibrium structural transitions in tRNA(Asp) transcripts. J. Am. Chem. Soc. *127*, 4659–4667.

Zwieb, C., van Nues, R.W., Rosenblad, M.A., Brown, J.D., and Samuelsson, T. (2005). A nomenclature for all signal recognition particle RNAs. RNA *11*, 7–13.